

## Quantifying lubricant droplet spreading on a flat substrate using molecular dynamics

Brooklyn Noble,<sup>1</sup> Andrey Ovcharenko,<sup>2</sup> and Bart Raeymaekers<sup>1,a)</sup>

<sup>1</sup>Department of Mechanical Engineering, University of Utah, Salt Lake City, Utah 84112, USA

<sup>2</sup>Western Digital Technologies Inc., San Jose, California 95138, USA

(Received 17 August 2014; accepted 3 October 2014; published online 13 October 2014)

Understanding the physical behavior of polymer-based lubricants on the nanoscale is of critical importance to a myriad of engineering applications and devices. We have used molecular dynamics simulations to quantitatively evaluate the physical mechanisms underlying perfluoropolyether lubricant spreading on a solid substrate. We quantify the effect of molecular mass, molecule length, and lubricant and substrate functional end groups on lubricant spreading. The results show that lubricant functional end groups play a critical role in lubricant spreading on the nanoscale. Lubricant spreading increases with increasing molecule length for lubricant with functional end groups, but decreases with the increase in molecule length for lubricant without functional end groups. In the former case, the fraction of the lubricant chain that is functional is the primary driving factor for lubricant spreading, while in the latter case, the molecular mass is most important. For both lubricants with and without functional end groups, spreading is inhibited by molecule entanglement beyond a critical molecule length, and spreading becomes independent of lubricant functional end groups and molecular mass. © 2014 AIP Publishing LLC.

[<http://dx.doi.org/10.1063/1.4898140>]

Understanding the physical behavior of polymer-based lubricants on the nanoscale is of critical importance to a myriad of engineering applications and devices, including micro and nanoelectromechanical systems (MEMS/NEMS),<sup>1</sup> machining,<sup>2</sup> and hard disk drives.<sup>3</sup> For instance, the functionality of many silicon-based MEMS/NEMS devices is dependent on mechanically interacting surfaces and, thus, the devices are subject to friction and wear. While used for its excellent electrical properties, the tribological properties of silicon are less favorable, and an ultra-thin lubricant film is often used to improve functionality and reliability of MEMS/NEMS devices. In hard disk drives, a monolayer of perfluoropolyether (PFPE) lubricant protects the diamond-like carbon overcoat and magnetic layer on the disk from contact and wear, improving the reliability of the interface between the recording head and the disk.<sup>3</sup> As the spacing between head and disk is reduced to increase the areal storage density,<sup>4</sup> the role of the lubricant layer becomes increasingly important. Hence, understanding the physical mechanisms of lubricant spreading on a flat substrate is essential to designing ultra-thin lubricant layers for nanoscale mechanical systems.

Both experimental and numerical studies have been documented in the literature, studying different aspects of lubricant spreading. Chen *et al.*<sup>5</sup> performed drag experiments of a recording head on hydrogenated disk samples and found that reducing the bonded ratio, i.e., the fraction of the lubricant that is bonded to the disk, enhances the durability of the head disk interface (HDI) due to the improved replenishment of mobile lubricant without functional end groups. Tani *et al.*<sup>6</sup> analyzed lubricant thickness of different polymer-based lubricants, after sliding a recording head on a disk, and

observed that lubricants with functional end groups exhibit considerable lubricant transfer from the disk to the head. Conversely, Ma *et al.*<sup>7</sup> used scanning microellipsometry to measure lubricant film thickness of lubricants with and without functional end groups, and observed that the functional end groups help lubricant retention at the HDI during sliding contacts. Brunner *et al.*<sup>8</sup> experimentally evaluated lubricant spreading of microsized PFPE lubricant droplets on a smooth substrate and noted that lubricant with functional end groups spread slower than lubricant without functional end groups. Mate<sup>9</sup> used a sharp needle to deposit droplets of various types of polymer-based lubricants onto a carbon-coated disk surface and also found that spreading kinetics slowed down for lubricant with increasing number of functional end groups. In addition, he documented an initial fast spreading mechanism when a central drop is present, and a slow spreading mechanism driven by the disjoining pressure gradient.

As experiments become increasingly difficult with decreasing length scale, numerical simulations have been used to study the interaction between lubricant and substrate on the nanoscale. Jhon *et al.*<sup>10</sup> used stochastic modeling techniques, validated with experiments, to demonstrate that polymer-based lubricants in the HDI exhibit increased mobility with decreasing molecular weight. This may result in changing lubricant surface morphology or lubricant transfer from the disk to the recording head. Coarse-grained bead spring (CGBS) molecular dynamics models<sup>10-22</sup> have been used to study the nanoscale dynamics of lubricant spreading. Researchers found that lubricant mobility decreases with increasing bonded ratio,<sup>11</sup> similar to what has been observed in experiments.<sup>5</sup> In addition, Guo *et al.*<sup>12</sup> demonstrated the formation of isolated islands of lubricant and a connected bridge network, while Ogata *et al.*<sup>13</sup> qualitatively showed that lubricant functional end groups form clusters of

<sup>a)</sup>Author to whom correspondence should be addressed. Electronic mail: bart.raeymaekers@utah.edu

lubricant. The molecular structure of the lubricant also plays a critical role in lubricant conformation and dynamics,<sup>14</sup> and Kremer and Grest<sup>15</sup> identified a critical entanglement length for a primitive lubricant chain.

Nanoscale droplet spreading of polymer-based lubricants has been of interest because the mechanism cannot simply be described by slippage of molecules along the substrate.<sup>16</sup> The Rouse model describes short molecule kinetics, and the reptation model describes long molecule kinetics.<sup>15</sup> Li *et al.*<sup>17,18</sup> modeled droplet spreading of PFPE lubricant on an amorphous carbon surface as a function of the lubricant functional end group and molecular weight, and qualitatively showed that lubricant without functional end groups forms a cap on the surface, whereas lubricant with functional end groups exhibits complicated terraced patterns during spreading, characterized by a foot, shoulder, and vertical step.

No publications seem to exist that quantitatively investigate the mechanisms underlying the complexities of nanoscale lubricant droplet spreading for polymer-based lubricants with and without functional end groups. This paper attempts to fill this gap, and uses a CGBS molecular dynamics model to quantify lubricant spreading of a nanoscale lubricant droplet on a flat substrate, as a function of polymer chain length, molecular mass, and functional end groups of the lubricant and the substrate.

We have performed simulations of a nanoscale polymer-based lubricant droplet spreading on a flat substrate using the LAMMPS code,<sup>23</sup> with a CGBS model that averages adjacent atomic interactions for computational efficiency, rather than considering each atom individually.<sup>19</sup> Figure 1(a) shows

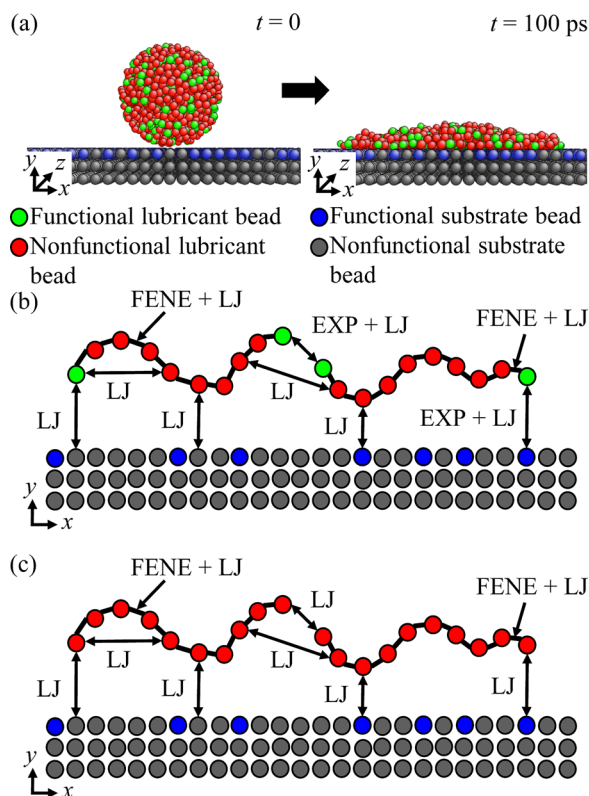


FIG. 1. (a) Schematic of the simulation showing the initial configuration at  $t=0$  and resulting configuration after lubricant spreading at  $t=100$  ps. (b) Schematic of coarse-grained bead spring model potential interactions for Zdol lubricant and (c) for Z lubricant.

a schematic of the model, which consists of a PFPE lubricant droplet that spreads on a rigid flat substrate. PFPE lubricants have a chemical structure of  $X-[(OCF_2CF_2)_p-(OCF_2)_q]-O-X$  ( $p/q \cong 2/3$ ). Here, two types of lubricant are considered; Zdol with functional end groups, i.e.,  $X = -CF_2CH_2OH$ , and Z without functional end groups, i.e.,  $X = -CF_3$ .<sup>7</sup> The substrate consists of a rigid bead lattice ( $35.0 \text{ nm} \times 35.0 \text{ nm} \times 2.1 \text{ nm}$ ), a fraction of which is functional to form an atomic bond with a lubricant functional end group. Figure 1(b) illustrates the CGBS model of a Zdol molecule, consisting of non-functional backbone beads with functional end beads. All potential functions and their parameters are similar to what others have previously used.<sup>20–22</sup> A truncated, shifted Lennard Jones (LJ) potential exists between all beads, except between the substrate beads, which are held rigid.

$$U_{LJ}(r) = 4\epsilon \left[ \left( \frac{\sigma}{r} \right)^{12} - \left( \frac{\sigma}{r} \right)^6 - \left( \frac{\sigma}{r_c} \right)^{12} + \left( \frac{\sigma}{r_c} \right)^6 \right], \quad (1)$$

where  $r$  is the distance between beads,  $\sigma = 0.7 \text{ nm}$  is the bead diameter,  $r_c = 2.5\sigma$  is the cutoff distance within which interactions between neighboring beads are considered, and  $\epsilon = Tk_B$  is the potential well depth, with  $T$  the absolute temperature and  $k_B$  the Boltzmann constant.<sup>20</sup> An exponential (EXP) potential is defined between functional beads

$$U_{EXP}(r) = -2\epsilon \exp\left(-\frac{r-r_c}{d}\right), \quad (2)$$

where  $d = 0.3\sigma$  is the characteristic short-range decay length.<sup>21</sup> In addition, a finitely extensible nonlinear elastic (FENE) potential simulates interactions between bonded neighbors of the PFPE lubricant chain

$$U_{FENE}(r) = -\frac{1}{2}kR_0^2 \ln \left[ 1 - \left( \frac{r}{R_0} \right)^2 \right], \quad (3)$$

where  $k = 30\epsilon/\sigma^2$  is the spring constant and  $R_0 = 1.5\sigma$  is the maximum extent of the bond.<sup>22</sup> Figure 1(c) shows the Z lubricant molecule. Since it has no functional end groups, Eqs. (1) and (3) fully describe its behavior. Periodic boundary conditions are employed in the  $x$  and  $z$ -directions to ensure that boundary effects do not interfere with lubricant spreading. However, the substrate is large enough such that lubricant does not cross any boundary during the simulation. The lubricant beads are free to move according to the microcanonical ensemble, and the model is maintained at 300 K using a velocity rescaling algorithm. 1000 lubricant beads, assembled into lubricant molecules of  $N$  beads, are initially placed in a 9 nm diameter spherical shell and equilibrated for 30 000 time-steps. Then, the lubricant droplet is released on the substrate and allowed to spread for 100 000 time-steps. A timestep of 1 fs is maintained throughout the entire simulation.

We have varied the lubricant molecule length  $1 \leq N \leq 100$  beads for both lubricant types, while maintaining a constant bead mass of 0.2 kg/mol, thus effectively varying the molecular mass. The functional fraction of the substrate  $0\% \leq S_f \leq 100\%$ , and the location of functional substrate beads is randomly selected. We quantify the

lubricant droplet spreading for each simulation by fitting the smallest circle diameter that encompasses every lubricant bead. Spreading as a function of time is also examined for each simulation. While the choice of potential functions and their constants can change the simulation results, we find that varying the interaction strength between two lubricant beads and between a lubricant and substrate bead changes the diameter of the spread lubricant droplet by less than 7%, for all practical cases.

We use a nondimensional diameter  $D/\sigma$ , where  $\sigma = 0.7$  nm is the bead diameter, to quantify the size of the lubricant droplet after it spreads on the flat substrate, measured after 100 ps when the droplet does not spread any further. Figure 2 shows the nondimensional diameter  $D/\sigma$  of a Zdol lubricant droplet as a function of the fraction of functional substrate beads  $S_f$  that can bond with the functional end beads of the lubricant, for lubricant molecules of different length  $N$ . The molecular mass increases with increasing molecule length  $N$  as the mass of each bead remains constant. Insets show three examples of top and side views of the droplet after spreading, for  $S_f = 50\%$ . Green beads indicate functional end beads and red beads indicate nonfunctional backbone beads of the Zdol lubricant. The top view also indicates the smallest circumscribed circle with diameter  $D$  around the spread lubricant. We observe that the fraction of functional substrate beads does not significantly affect spreading of lubricant with functional end beads, indicating that the interaction of the Zdol lubricant with other lubricant molecules plays a more dominant role than the interaction with the substrate. We also observe that lubricant spreading increases with increasing molecule length. However, beyond  $N = 20$ , the diameter of the spread lubricant droplet remains almost constant, independent of  $N$ . Although it is documented that molecules of increased molecular mass exhibit decreased mobility,<sup>10</sup> here the presence of functional end beads of the lubricant is the dominant mechanism with respect to lubricant spreading, since shorter

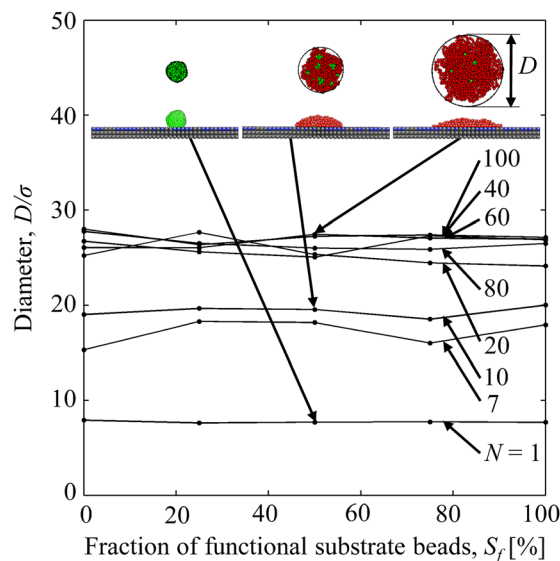


FIG. 2. Spreading diameter of Zdol lubricant as a function of the fraction of functional substrate beads  $S_f$  and lubricant molecule length  $N$ . Insets show three examples of top and side views of lubricant droplets after spreading.

molecules exhibit less mobility. In the limit case when  $N = 1$ , the lubricant consists entirely of functional end beads and the attractive exponential potential dominates lubricant spreading. One large cluster of lubricant is formed on the substrate because all beads bond to each other, and lubricant spreading is inhibited. When  $N = 10$ , the fraction of functional lubricant end beads represents that 20% of all lubricant beads and mobility and spreading are increased. While the functional end beads still bond together as observed by the (green) clusters of functional end beads in the middle inset of Fig. 2, the nonfunctional backbone beads experience increased mobility because LJ-interactions between the lubricant and substrate drive spreading. The side view of this example suggests a stepped formation.<sup>17</sup> For  $N = 100$ , the fraction of functional end beads represents only 2% of all lubricant beads and spreading is greatly increased. Several lubricant end bead clusters are formed, but a long chain of backbone beads enables mobility. The side view of this example demonstrates increased conformation with the substrate. Thus, mobility increases with decreasing lubricant bonded ratio, which is consistent with the results of Chen *et al.*<sup>5</sup> and Tani *et al.*<sup>6</sup>

Figure 3 shows the nondimensional diameter  $D/\sigma$  of a Z lubricant droplet as a function of the fraction of functional substrate beads  $S_f$ , for lubricant molecules of different length  $N$ . Insets show three examples of top and side views of the droplet after spreading, for  $S_f = 50\%$ . We observe that the fraction of functional substrate beads does not affect spreading of lubricant without functional end beads, which is expected since the lubricant cannot bond to the substrate. In the limit case of  $N = 1$ , large lubricant mobility is observed as no bonding or entanglement of the polymer inhibits spreading. Spreading decreases with increasing molecule length  $N$ . However, when the lubricant molecule length increases beyond  $N = 20$ , the diameter of the lubricant droplet remains almost constant, independent of  $N$ . Clusters of lubricant end beads are not formed since there are no

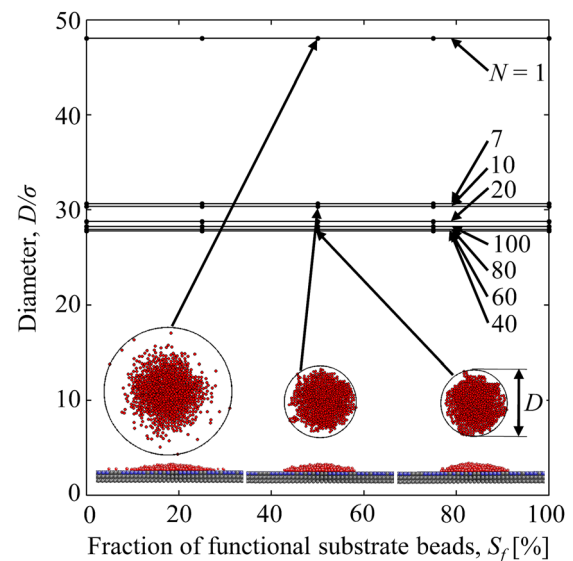


FIG. 3. Spreading diameter of Z lubricant as a function of the fraction of functional substrate beads  $S_f$  and lubricant molecule length  $N$ . Insets show three examples of top and side views of lubricant droplets after spreading.

functional lubricant end beads, resulting in drastically different spreading behavior than for Zdol lubricant. This is illustrated in the side views of the cases of  $N = 10$  and  $N = 100$ , which show the formations of a cap, similar to observations in simulations by Li *et al.*<sup>17</sup>

Figure 4 shows four examples of lubricant spreading with beads of one molecule depicted in the same color, and end beads indicated with an additional black circle. For Zdol lubricant of length  $N = 10$ , clumping of the functional end beads of the molecules is observed, inhibiting lubricant mobility. The magnified inset shows that the nonfunctional backbone beads form loops that orient away from the end bead clusters, driven by LJ interactions with the substrate. The geometry of the loops and mobility of the lubricant is restricted by the molecule length and by proximity to other molecules. When  $N = 100$ , we observe clusters of functional end beads without loop formations of nonfunctional backbone beads. The long chains of backbone beads cross each other and entangle, severely inhibiting mobility. For  $N > 20$ , lubricant molecule entanglement is the dominant mechanism that determines spreading of the lubricant, which agrees with the simulated polymer melt results of Kremer *et al.*<sup>15</sup> Thus, as observed in Fig. 2, the diameter of the lubricant drop is independent of the molecule length when  $N > 20$ . For Z lubricant of length  $N = 10$ , clusters are not observed because there are no functional end beads. Thus, both end beads and backbone beads exhibit mobility, resulting in greater spreading than the Zdol lubricant. The magnified inset shows that some molecules even detach from the main lubricant droplet. For  $N = 100$ , the spreading result is similar to that of Zdol lubricant with  $N = 100$  except that no clusters are formed. Spreading is inhibited as a result of entanglement. While it is documented in the literature that mobility decreases with increased molecular mass,<sup>9</sup> we note that beyond  $N = 20$ , molecule entanglement is the dominant factor that inhibits

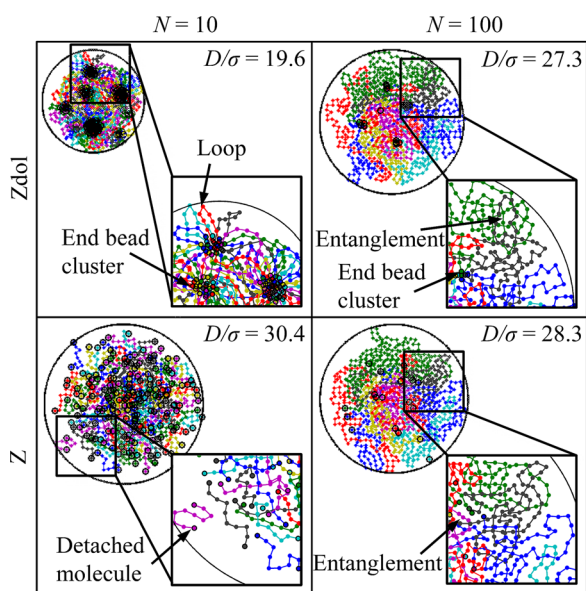


FIG. 4. Top view of lubricant spreading of Zdol and Z lubricants with lubricant molecule length of  $N = 10$  and  $N = 100$ , illustrating the physical mechanisms that drive lubricant spreading. Beads of the same molecule are displayed in the same color, and end beads are indicated with an additional black circle. Insets show a magnified view.

mobility. We have also performed simulations in which the molecular mass is held constant for different molecule length, i.e., by changing the bead mass, confirming this observation.

Figure 5 shows the nondimensional diameter  $D/\sigma$  of a Zdol and Z lubricant droplet as a function of time for  $N = 1, 7, 100$ , and  $S_f = 50\%$ . Spreading time is calculated from releasing the droplet until its diameter does not change by more than 4%, indicated with an additional blue circle. The spreading time is related to the diameter of the lubricant droplet after spreading. For instance, when  $N = 1$ , spreading of the droplet finished after 30 ps for Zdol compared to 75 ps for Z lubricant, because the extreme mobility of the Z lubricant with  $N = 1$  results in a diameter of the droplet on the substrate that is approximately five times larger than the corresponding Zdol case, which shows maximum clumping. We note that for  $1 \leq N \leq 20$ , the spreading time increases with increasing  $N$  for Zdol, because a decreased fraction of functional lubricant beads increases mobility. In contrast, spreading time of Z lubricant decreases with increasing  $N$ , because the increased molecular mass decreases mobility. When  $N > 20$ , entanglement dominates lubricant spreading for both Zdol and Z lubricants, and spreading time is almost independent of  $N$ . However, when comparing molecules of identical length, Z lubricant always spreads further than Zdol lubricant, because the latter bonds with functional beads on the substrate, which decreases mobility. We observe that spreading occurs fast when a central drop is present and subsequently slows down, similar to the experimental findings of Mate,<sup>9</sup> although the time and length scales of molecular dynamics simulations versus experiments are drastically different due to the intrinsic limitations of the simulations.

The simulations show that lubricant functional end groups play a critical role in lubricant spreading. The fraction of functional end groups decreases with increasing molecule length, which increases spreading because lubricant mobility is less restricted by bonding between the functional

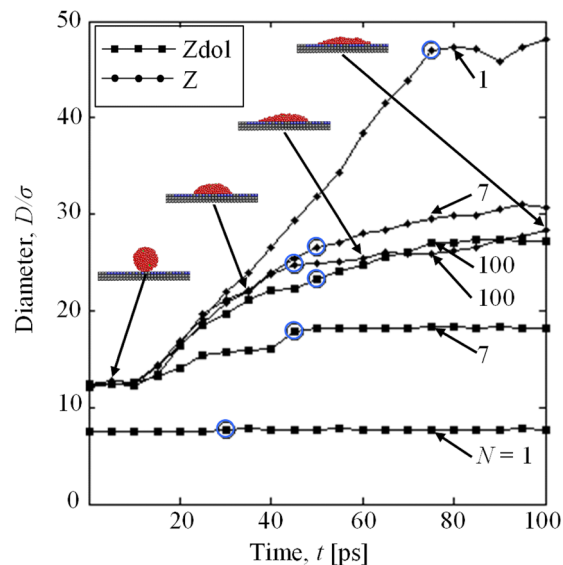


FIG. 5. Spreading diameter as a function of time for Z and Zdol lubricants of molecule length  $N = 1, 7$ , and  $100$ , for  $S_f = 50\%$ . Spreading time is indicated with an additional blue circle for each simulation, and insets show side views of Z lubricant,  $N = 100$  at four points in time.

end groups of different molecules. For lubricant without functional end groups, spreading decreases with increasing molecule length because the molecular mass increases. Spreading is always dominated by molecule entanglement beyond a critical molecule length ( $N=20$  in our simulations).

The authors gratefully acknowledge support from Western Digital Technologies Inc. for this work, and Dr. Min Yang for her interest in this research. We thank Michael Price for helpful discussions. Brooklyn Noble also acknowledges support from a University of Utah Undergraduate Research Opportunity (UROP) Award.

<sup>1</sup>K. C. Eapen, S. T. Patton, and J. S. Zabinski, *Tribol. Lett.* **12**, 35 (2002).

<sup>2</sup>V. A. Godlevshi, A. V. Volkov, V. N. Latyshev, and L. N. Maurin, *Lubr. Sci.* **9**, 127 (1997).

<sup>3</sup>A. Khurshudov and R. J. Waltman, *Wear* **251**, 1124 (2001).

<sup>4</sup>R. Wood, *J. Magn. Magn. Mater.* **321**, 555 (2009).

<sup>5</sup>C.-Y. Chen, D. Bogy, and C. S. Bhatia, *Tribol. Lett.* **10**, 195 (2001).

<sup>6</sup>H. Tani, K. Iwasaki, Y. Maruyama, I. Ota, and N. Tagawa, *IEEE Trans. Magn.* **47**, 1837 (2011).

<sup>7</sup>X. Ma, J. Gui, L. Smoliar, K. Grannen, B. Marchon, M. S. John, and C. L. Bauer, *J. Chem. Phys.* **110**, 3129 (1999).

<sup>8</sup>R. Brunner, I. Etsion, and F. E. Talke, *Langmuir* **26**, 1824 (2010).

<sup>9</sup>C. M. Mate, *Tribol. Lett.* **51**, 385 (2013).

<sup>10</sup>M. S. Jhon, S. Izumisawa, Q. Guo, D. M. Phillips, and Y.-T. Hsia, *IEEE Trans. Magn.* **39**, 754 (2003).

<sup>11</sup>S. K. Deb Nath, C. H. Wong, V. Sorkin, Z. D. Sha, Y. W. Zhang, and S. G. Kim, *Tribol. Trans.* **56**, 255 (2013).

<sup>12</sup>Q. Guo, H. Chen, B. C. Smith, and M. S. Jhon, *J. Appl. Phys.* **97**, 10P301 (2005).

<sup>13</sup>S. Ogata, Y. Mitsuya, H. Zhang, and K. Fukuzawa, *IEEE Trans. Magn.* **41**, 3013 (2005).

<sup>14</sup>H. Chen, Q. Guo, and M. S. Jhon, *IEEE Trans. Magn.* **43**, 2247 (2007).

<sup>15</sup>K. Kremer and G. S. Grest, *J. Chem. Phys.* **92**, 5057 (1990).

<sup>16</sup>V. M. Samsonov and A. S. Ratnikov, *Colloids Surf., A* **298**, 52 (2007).

<sup>17</sup>X. Li, Y. Hu, and H. Wang, *J. Appl. Phys.* **99**, 024905 (2006).

<sup>18</sup>X. Li, Y. Hu, and H. Wang, *J. Appl. Phys.* **100**, 074901 (2006).

<sup>19</sup>Q. Guo, S. Izumisawa, D. M. Phillips, and M. S. Jhon, *J. Appl. Phys.* **93**, 8707 (2003).

<sup>20</sup>D. Pan, A. Ovcharenko, R. Tangaraj, M. Yan, and F. E. Talke, *Tribol. Lett.* **53**, 373 (2014).

<sup>21</sup>Y. Li, C. H. Wong, B. Li, S. Yu, W. Hua, and W. Zhou, *Soft Matter* **8**, 5649 (2012).

<sup>22</sup>T. Yi, U. S. Ramasamy, S. Lichter, and A. Martini, *Tribol. Lett.* **54**, 119 (2014).

<sup>23</sup>S. Plimpton, *J. Comput. Phys.* **117**, 1 (1995).